International Journal of Engineering and Geosciences

https://dergipark.org.tr/en/pub/ijeg

e-ISSN 2548-0960

Evaluating the performance of machine learning algorithms in monitoring temporal changes in land cover and land use in mountainous areas: The Ourika basin as a case study

Ouguinaz Abdelkarim [1], Jellouli Amine [2], Okacha Abdelmounaim [3], Chakouri Mohcine [2], Chouidda Hasnaa [2]

[1] Abdelmalek Essaâdi University, Research Group on Geography and Development, Morocco, abdelkarim.ucam@gmail.com
[2] Sultan Moulay Slimane University, Geomatics, Georesources and Environment Laboratory, Morocco, a.jellouli@usms.ma
[2] Sultan Moulay Slimane University, Geomatics, Georesources and Environment Laboratory, Morocco, chakouri.mohcine@gmail.com
[2] Sultan Moulay Slimane University, Data4Earth Laboratory, Morocco, ha.chouidda89@gmail.com
[3] Cadi Ayyad University, Geomorphology, Environment & Society Laboratory, Morocco, a.okacha@uca.ac.ma

Cite this study: Ouguinaz, A., Jellouli, A., Okacha, A., Chakouri, A., & Chouidda, H. (2026). Evaluating the performance of machine learning algorithms in monitoring temporal changes in land cover and land use in mountainous areas: the Ourika Basin as a case study. International Journal of Engineering and Geosciences, 11 (3), 732-748.

https://doi.org/10.26833/ijeg.1811922

Keywords
Remote Sensing
LULC classification
Google Earth Engine
Machine learning
Change detection

Research Article

Received: 27.10.2025
Revised: 02.01.2026
Accepted: 26.01.2026
Published: 01.10.2026

Abstract

Changes in land use and land cover (LULC) represent a major environmental challenge resulting from rapid population growth, necessitating accurate monitoring and assessment of their impacts. This study aims to evaluate the effectiveness of three machine learning algorithms, namely Support Vector Machines (SVM), Decision Trees (CART), and Random Forests (RF), in classifying land cover patterns and land use in the Ourika Mountain Basin for the periods 1987 and 2025 using Landsat 5 TM and 9 OLI satellite data via Google Earth Engine (GEE). The results showed a clear superiority of the random forest (RF) algorithm in terms of accuracy and consistency, as it recorded the highest values for overall accuracy (OA) and kappa coefficient (KC) for both years, with an overall accuracy of 93% and a kappa coefficient of 0.91 for 1987, and increased to 95% and 0.94, respectively, for 2025. Based on these results, the classification map produced by the RF algorithm was adopted for temporal change analysis. The change analysis revealed significant environmental shifts, represented by a notable decline in natural areas of forests and pastures by 10% of the total area of the basin (equivalent to 5831 hectares). In contrast, there has been a steady expansion in agricultural land, urban areas, and bare land. These changes highlight the increasing human pressures that are contributing to the acceleration of environmental degradation within the Ourika basin. This study provides an effective methodology for monitoring temporal changes and analyzing environmental transformations and can be a valuable tool to support natural resource management and the development of effective strategies for environmental planning and sustainable management of natural resources in similar mountainous areas.

1. Introduction

Remote sensing is one of the most important technologies used in LULC detection, as it is effective for local and regional scale mapping. Among its advantages is that it provides detailed mapping of the terrain in a short time and at low cost. In addition, it provides synoptic mapping of the terrain, which allows for the collection of a diverse database consisting of satellite imagery, GIS data, thematic maps, etc. Classification methods are among the most widely used methods in remote sensing for mapping and monitoring LULC changes in a given study area. Continuous and accurate analysis of LULC is an integral part of sustainable development activities. LULC maps are a fundamental input in most scientific studies related to urban and regional planning [1, 2], climate change [3, 4], water resources [5], geomorphology [6], agricultural land monitoring [7, 8], and natural disaster and risks monitoring [9, 10]. In general, they can assist in watershed management studies, as accurate and important sources of information for natural resource managers, forest monitoring programs, and the development of integrated resource management

strategies [11–13]; and decision-making related to environmental management and future planning [10, 14–18].

The advent of remote sensing and GIS technologies has precipitated a paradigm shift in the realm of land use change (LUC) research, bestowing unparalleled prowess in the domains of data collection, storage, analysis, and visualization[2]. The utilization of these instruments furnishes a malleable framework for the identification of alterations in land utilization through the passage of time. This is predominantly attributable to the accessibility of remote sensing imagery and the analytical prowess of machine learning algorithms [19].

Machine learning is a component of artificial intelligence, although it seeks to solve problems based on historical or previous examples [20]. It involves designing systems capable of learning from data without explicit programming, by improving their performance in specific tasks with increased exposure to experience [21]. In addition, it involves developing algorithms and techniques rather than programming the performance of functions [20], and it became a relatively new scientific field, and is under continuous development [22]. Machine learning algorithms can be either supervised or unsupervised, while some authors also classify other algorithms as reinforcement learning, because these technologies learn data and identify patterns for the purpose of interacting with the environment [23].

Supervised learning relies on pre-classified data, where each example has associated inputs and outputs. The main goal is to build a model capable of predicting outputs for new, previously unseen data. Its most prominent techniques include linear and logistic regression, random forests, support vector machines, and neural networks [23, 24]. In unsupervised learning, there is no teacher available. Instead, it relies solely on information variables [25]. It is a method of absorbing information without guidance [20], searching for similarities between data to determine the possibility of classifying them into named groups. For example, in remote sensing, unsupervised methods such as partitioning and merging, Isodata, K-means, FCM, neural network-based methods, and scale space techniques are commonly used [24, 26].

Several studies have addressed the consequences of land use change over time. The impact of this change varies from one location to another; it depends on geographical location and scale, leading to the degradation of ecosystems in many sites studied around the world. Zhang et al (2016) revealed how land use change in the Heihe River Basin in northwestern China led to slight decreases in surface runoff, groundwater discharge, and water flow [13]. Cohen et al (2016) reported forest disturbance across the United States between 1985 and 2012, with national disturbance rates ranging from 1.5 to 4.5% of forest area annually. They linked this to the forest harvest cycle in forested areas [27]. Rahman et al (2020) analyzed the performance and accuracy of different machine learning algorithms on three different classifications of spatial and multispectral satellite images (Landsat-8, Sentinel-2, and Planet images) to classify urban and rural areas in Bangladesh [28]. El Moussaoui et al (2025) evaluated the performance of supervised methods (support vector machines, maximum likelihood, and minimum distance) and the unsupervised classification method (Isodata) for mapping argan forests in the Smimou of the Essaouira province, in addition to examining the impact of the resampling method and digital elevation model (DEM) integration on the results of this classification [29]. A range of studies have highlighted the direct link between land use changes and land surface temperature (LST), with urban areas showing significantly higher mean temperatures than vegetated or aquatic areas[18, 30, 31]. El Malki et al (2021) monitored and measured land degradation dynamics and improved land use maps in the Ourika basin between 1987 and 2019, where Landsat 5 and 8 images were classified and processed using a support vector machine (SVM) algorithm in QGIS software [32]. Fast-growing population and increased socio-economic needs are putting pressure on LULC in the Ourika Basin. This pressure leads to unplanned and often uncontrolled changes in land use, which often result in poor management of agricultural, residential, pasture, and forest lands, leading to serious environmental problems such as soil erosion, landslides, floods, and others.

The novelty of this work lies in the diachronic comparative analysis (between 1987 and 2025) of the performance of Random Forest, SVM, and CART classification methods coupled with spectral indices applied to different generations of Landsat sensors, allowing the impact of radiometric, spectral, and spatial characteristics on classification accuracy. Furthermore, it emphasizes the robustness of the algorithms in an ecologically vulnerable mountainous area with spectrally similar classes. Moreover, the study area had not been the subject of sufficient research in the Ourika watershed. It provides a methodological framework for the long-term monitoring of LULC that is capable of being reproduced. This framework is based on multi-sensor Landsat archives, and it assists decision makers in the field of environmental planning in this study area, as well as in other similar fields.

In this study, we will evaluate the suitability of machine learning algorithms such as classification and regression trees (CART), support vector machines (SVM), and random forest (RF) for land cover classification in the complex Ourika Mountain Basin, which is characterized by dense land cover and limited class separability. Factors such as rugged topography, seasonal snow cover, and terrain-induced shadows further increase the difficulty of land cover distinction and classification. This evaluation will be conducted using Landsat 5 TM and Landsat 9 OLI-2 images processed through cloud computing techniques within the Google Earth Engine (GEE) platform. In order to enhance the accuracy of this classification, we will incorporate a set of spectral indices such as the Normalized Difference Vegetation Index (NDVI), Normalized Difference Build-up Index (NDBI), Bare Soil Index (BSI), and Enhanced Vegetation Index (EVI), and elevation and slope criteria. These classification algorithms were chosen because of their large use in

LULC mapping, and have not been applied and compared yet in this basin.

2. Materials and Method

2.1. Study area

The Ourika basin is located in the High Atlas Mountains (south of Marrakesh), between 31° 31' 21" north latitude and 7° 30' 60" west longitude (Figure 1). It is delimited to the south by the high basins of the Souss and Draa, to the west by the Ghighaya and Issil basins, to the east by the Zat and Gandji basins, and to the north by the El Haouz plain.

The main river originates in the foothills of the High Atlas Mountains. It is located in a catchment area that rises to 4001 meters (Mount Ifghane) and exits at an altitude of 1070 meters at the end of the Atlas Mountains. The basin is characterized by steep slopes and impermeable, compact rock formations [33].

From a geological and lithological point of view, the basin is characterized by two distinct lithological facies. The first one, which dominates the upper part of the basin, is composed primarily of volcanic and metamorphic formations, including pink granite, Toubkal andesite, and migmatite rocks. This unit accounts for approximately 61% of the total basin area. The second facies, occupying the lower levels of the basin, is represented by softer to moderately consolidated lithologies, mainly Permian–Triassic and Quaternary sedimentary deposits, covering about 39% of the basin [34, 35].

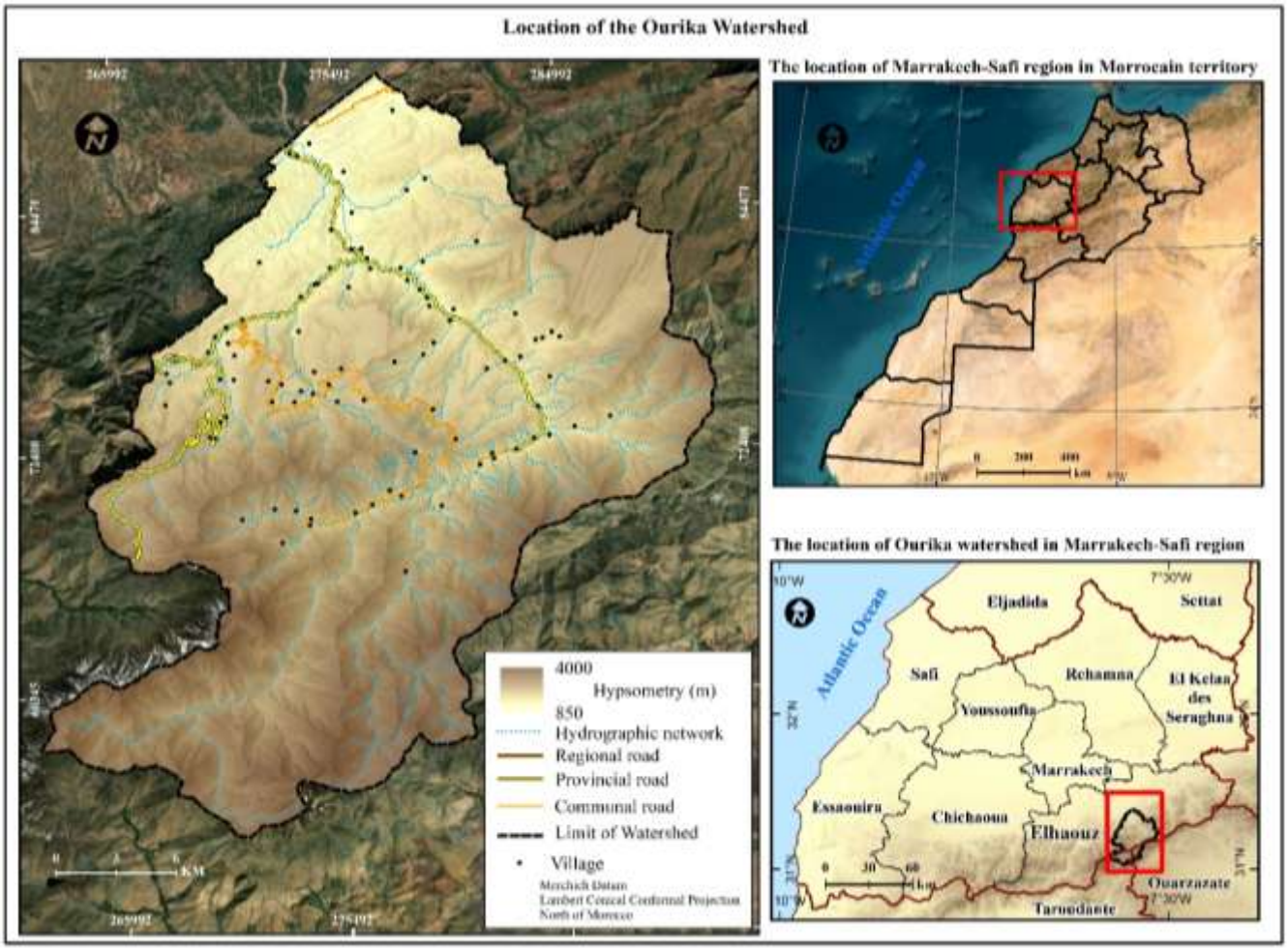

Figure 1. Location and position of the Ourika watershed

Furthermore, the lithological composition of layers gives rise to a diversity of soil types. As outlined in several studies, crystalline and fissured soils typically develop over volcanic formations, whereas semi-permeable soils are predominantly associated with formations of Triassic red clays, schist, flysch, granite, and basalt. In contrast, permeable soils are largely formed on limestone, basalt, and silt deposits [33, 35].

The Ourika watershed is characterized by a semi-arid to semi-humid climate, marked by spatial and temporal variability. Rainfall exhibits strong heterogeneity in relation to altitude, intensity, and geographic distribution. The mean annual rainfall recorded at the Aghbalou station was approximately 541 mm, with values increasing progressively with elevation and exceeding 700 mm per year at the highest peaks of the watershed [33]. In parallel, Temperatures within the Ourika watershed exhibit marked variability, ranging from −7.2°C during the coldest periods to 48.2°C during extreme summer conditions, with an average annual value of approximately 27.8°C [36]. Additionally, the average maximum temperatures fluctuate between 21.5°C and 32°C, while minimum values range from 4°C to 5.7°C. July and August represent the hottest months of

the year, whereas December and January correspond to the coldest months [37].

The main activities within the watershed include grazing, agriculture, and a booming tourism sector, all of which exert significant pressure on natural resources and lead to widespread changes in the landscape, along with phenomena such as soil degradation, deforestation, natural disasters, rigorous exploitation of natural resources, inadequate infrastructure, and social and economic deprivation.

These dynamics have resulted in profound changes in land use patterns within the basin, particularly affecting traditional agro-pastoral systems, notably the Agdal system, which has seen a gradual decline in its regulatory and environmental functions. As a result of the transformation of production systems, the expansion of agriculture within some meadows, and the growth of commercial tree plantations in irrigated areas at the expense of subsistence production, the pastoral domain has shrunk, livestock breeding has declined, and long-term transhumance patterns have been gradually abandoned. These trends have been observed, to varying degrees, in different regions of the Atlas Mountains, including the Ourika watershed. Hence, it is important to analyze land cover and land use changes within the basin with the utmost precision, relying on machine learning methodologies capable of capturing these complex and interrelated transformations

2.2. Satellite data

Remote sensing data significantly enhance our contemporary understanding of the local and global scale changes in LULC and its applications due to their wide synoptic view and periodic monitoring of the Earth's surface [38]. This research used Landsat 5 and 9 image datasets with a spectral range covering the visible, near-infrared, and shortwave infrared regions. This data image was specifically chosen based on its broad use, open and free accessibility to its products, and its spatial, spectral, and temporal characteristics, which are suitable for studying LULC change.

For the first dataset, Landsat 5 Level 2 Group 2 Class 1 data represent the best processed version of Landsat 5 satellite images covering the period from 1984 to 2012. They provide accurate surface reflectance for the optical bands after applying atmospheric correction, as well as a separate surface temperature product. It has been processed within Group 2 using the latest algorithms and global atmospheric models, ensuring high consistency in geometric and radiometric accuracy with recent Landsat 8 and 9 data [4].

As well, the Landsat 9 Level 2 Group 2 Class 1 dataset represents the latest and most accurate Earth observation products from the Landsat program. This data image is collected by the Operational Land Imager-2 sensor for optical bands and the Thermal Infrared-2 sensor for thermal bands. Thus, the data is processed into surface reflectance for optical bands and surface temperature for thermal bands after applying advanced atmospheric corrections via the LaSRC algorithm using modern climate models [39]. The data were classified as Group 2, ensuring full reliability in calibration and geometric accuracy. Its quality and reliability with previous generations enable researchers to monitor historical environmental changes over three decades, such as deforestation, urban expansion, and water body decline. It also supports vital applications such as crop monitoring, water resource management, forest and ecosystem health assessment, and climate studies, as it offers good spatial and spectral resolution [4]. The (Table 1) presents the spatial and spectral characteristics of the different optical and thermal bands of Landsat 5 and 9 data.

Table 1. The spatial and spectral characteristics of Landsat 5 and 9 data [40]

Parameter	Landsat 5 (TM)	Landsat 9 (OLI-2)
Spatial Resolution	**30 meters** for most bands	**30 meters** for most bands
Temporal Resolution	16 days	16 days (8 days when combined with Landsat 8)
Number of Bands	7 bands	9 bands (11 with thermal bands from TIRS-2)
Band 1 - Coastal/Aerosol	Not Available	**0.433–0.453 µm (30 m)**
Band 2 - Blue	0.45–0.52 µm (**30 m**)	0.450–0.51 µm (**30 m**)
Band 3 - Green	0.52–0.60 µm (**30 m**)	0.53–0.59 µm (**30 m**)
Band 4 - Red	0.63–0.69 µm (**30 m**)	0.64–0.67 µm (**30 m**)
Band 5 - Near-Infrared (NIR)	0.76–0.90 µm (**30 m**)	0.85–0.88 µm (**30 m**)
Band 6 - Short-Wave IR (SWIR) 1	1.55–1.75 µm (**30 m**)	1.57–1.65 µm (**30 m**)
Band 7 - Short-Wave IR (SWIR) 2	2.08–2.35 µm (**30 m**)	2.11–2.29 µm (**30 m**)
Band 8 - Panchromatic	Not Available	**0.50–0.68 µm (15 m)**
Band 9 - Cirrus	Not Available	**1.36–1.38 µm (30 m)**
Thermal Band(s)	Band 6: 10.40–12.50 µm (**120 m**, resampled to 30 m)	TIRS-1: 10.60–11.19 µm (**100 m**, resampled to 30 m)
		TIRS-2: 11.50–12.51 µm (**100 m**, resampled to 30 m)

Other supplementary data include the NASA Digital Elevation Model (NASADEM) with a spatial resolution of 30 meters. This product offers significant improvements in vertical accuracy and topographic reliability, especially in areas with rugged terrain. It is processed and provided by the United States Geological Survey (USGS) through platforms such as Earth Explorer[41].

2.3. Methodology

The adoption and wide use of RF, SVM, and CART algorithms have grown with the expansion of computing resources and the availability of diverse datasets, particularly in the fields of remote sensing. As one of the oldest structured decision tree algorithms, CART has maintained a strong presence due to its interpretability and ease of generating decision rules [42], which helps domain experts understand the model's outputs. Its simplicity has made it particularly popular in applications where transparency is of paramount importance [43].

The SVM algorithm has gained widespread popularity thanks to its solid theoretical foundation and proven effectiveness in processing complex, multidimensional data, which is common in remote sensing and image processing. Its ability to process linearly inseparable data through kernels has made it a preferred tool in many fields, such as crop classification and urban build-up mapping, where data is highly complex [44–46].

The RF algorithm emerged as an advanced computational technique, providing solutions to some of the overfitting problems in CART by combining multiple trees [47, 48]. It quickly gained widespread popularity in various applications due to its robustness and excellent classification accuracy [17], and low parameter tuning requirements. In the field of remote sensing, RF technology has been widely praised for its performance in classifying satellite images and land cover, outperforming traditional classifiers that do not require fine-tuning of parameters [49].

Obtaining an accurate thematic map necessarily requires the selection of a suitable classification algorithm, which depends mainly on the user's experience and level of knowledge, as well as on the algorithm's ability to classify land cover correctly, its operational capacity, interpretability, and transparency [50]. Training samples, classifiers, and auxiliary data are considered to be the main determinants affecting the accuracy of supervised land cover classification [51]. Several studies have been conducted to evaluate the accuracy of different classifiers [46, 52–55]. Others have delved deeper into the use of various ancillary data [50, 56–58]. Classification accuracy can be improved by using excellent classifiers with sufficient auxiliary data, and the most obvious approach to increasing classification accuracy remains providing sufficient, high-quality training samples [57, 59–61].

This study relied on three main sources to compile the reference samples: fieldwork, high-resolution (2 m) Google Earth imagery, and national forest inventory data. These sources accounted for 55%, 30%, and 15% of the total sample, respectively. A comprehensive reference database was created, comprising 1240 representative samples, selected in a stratified randomized method across different land cover classes. This represented the entire sample set before it was split. The data were then divided into a training set (70%) and an independent validation set (30%). The validation set was used to evaluate the accuracy of the produced land cover classification maps [62]. To minimize spatial bias in the evaluation process, the validation samples were kept spatially independent of the training samples.

The GEE engine is a rapid analysis platform. Its use of Google's computing infrastructure provides online access to Landsat data archived as a dataset by the US Geological Survey [63–66]. All Landsat data processing in this work was performed using cloud computing technology on the GEE platform (Figure 2).

As a first step, the Shapefile defining the perimeter of the Ourika watershed was imported into GEE to facilitate the filtering, cropping, classification, and analysis of Landsat 5 and 9 images within the specified geographic parameters. To ensure data integrity and surface feature clarity, images with low cloud cover (less than 10%) were selected [8].

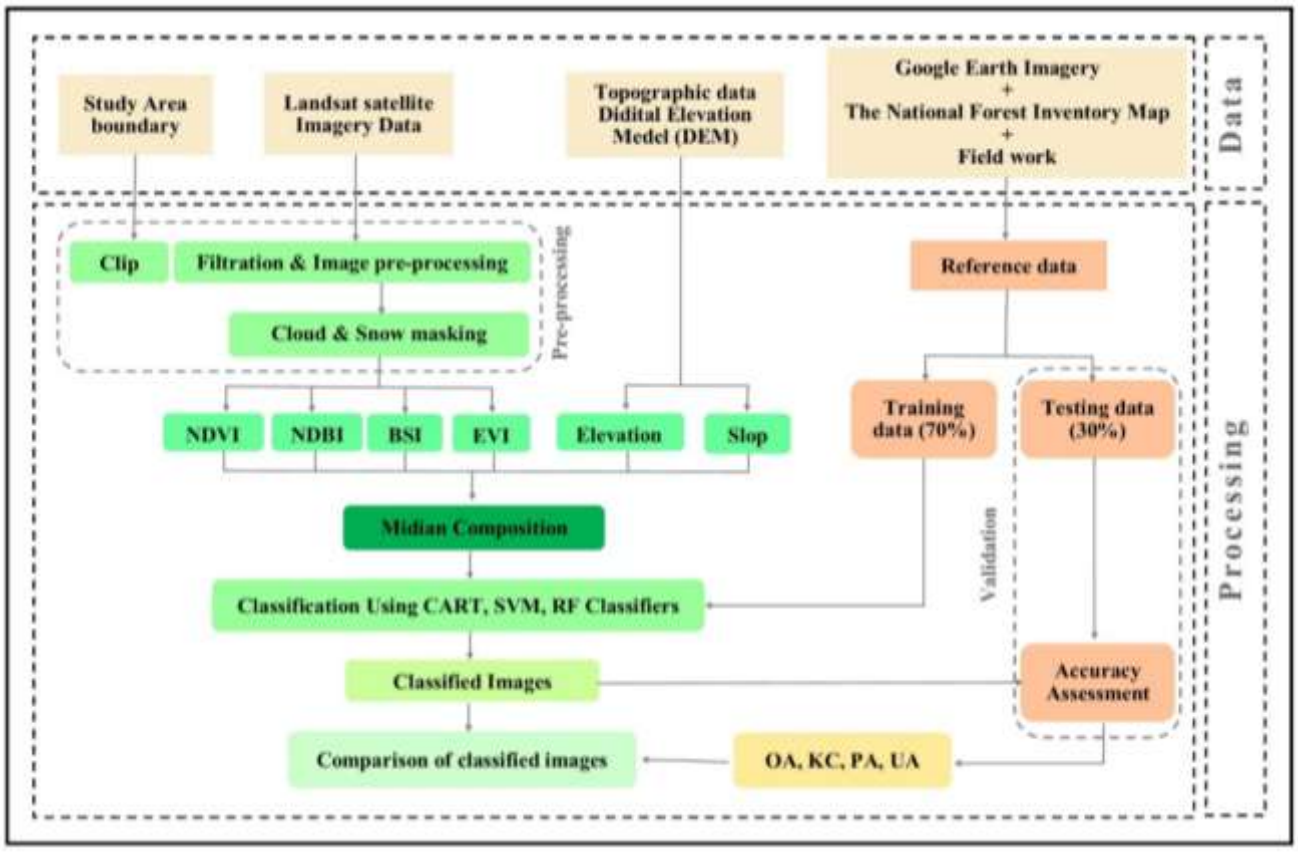

Figure 2. Methodology for land cover classification in the Ourika watershed on the GEE

Before starting to classify the images, the data was pre-processed by correcting first for surface reflectance using measurement coefficients provided by the US Geological Survey (USGS) to convert digital number (DN) values to actual reflectance measurements. Secondly, pixel quality assessment (QA_PIXEL) was used to separate pixels at risk due to cloud interference or shadow effects. The Natural Difference Snow Index (NDSI) was also calculated, and pixels exceeding a threshold of 0.4 were discarded to ensure that the dataset was not biased by snow [67].

In order to increase classification accuracy, a set of spectral indices was calculated to facilitate the distinction between different land cover categories. These indices were included to enhance the dominant spectral components in the study area, particularly vegetation cover, build-up areas, and bareland, which cover large areas of the Ourika Basin. Their inclusion in the classification algorithms also improves the separability between classes and reduces spectral overlap between them, which positively affects the accuracy of land use and land cover classification. These indices included the Normalized Difference Vegetation Index (NDVI) for vegetation cover [30, 68, 69], the accumulated normal difference index for build-up areas (NDBI) [30, 70], the Bare Soil Index (BSI) for arid lands [71], and the Enhanced Vegetation Index (EVI) for dense vegetation cover [8, 72, 73]. Furthermore, topographic data derived from the NASADEM elevation model [59, 74–77], including slope metrics [78], were used to enhance classification accuracy within the rugged terrain of the Ourika watershed. Training samples were carefully collected using the fieldwork, Google Earth imagery, and national forest inventory data, and classified into five main categories: forests, build-up areas, agricultural fields, bare land, and pastures. Water bodies are minimal to non-existent and were therefore excluded from the classification. Training was performed separately using the three classifiers of RF, SVM, and CART.

Finally, the accuracy of the classification was evaluated using confusion matrix metrics, overall accuracy, kappa coefficient, producer accuracy, and user accuracy to verify the reliability of the results and the efficiency in discriminating between different LULC classes.

3. Results and Discussion

3.1. LULC classification

A visual assessment of the classification maps presented in (Figure 3) reveals a common pattern in the accuracy of representation of different categories, regardless of the performance of each classifier.

The classification results indicate that the most distinguishable land cover categories are forests, agricultural areas, bare land, and pastures. This is especially true for RF, which correctly classified all areas corresponding to these land covers, particularly in 2025. The Random Forest (RF) classifier significantly outperformed the others in the accuracy of classifying these categories, showing particularly accurate performance in distinguishing them for the year 2025.

Conversely, low-density build-up areas posed the greatest challenge in the classification process, especially for the CART and SVM algorithms. There was some

confusion between bareland and build-up areas, with some being misclassified due to the similarity in spectral characteristics between the two land covers. This similarity is attributed to the use of local materials in housing construction, which makes their spectral reflections similar to those of bareland.

In the 1987 imagery, minor classification errors were also observed with the CART and SVM classifiers, where limited areas of forest were classified as agricultural areas. This can be explained by the similarity in spectral reflections resulting from the density of crops, which closely mimics that of regenerated forest cover. Similarly, some seasonal vegetation categories with similar spectral behavior, such as arable land planted with cereals and pasture land, overlapped, leading to a decline in discrimination accuracy.

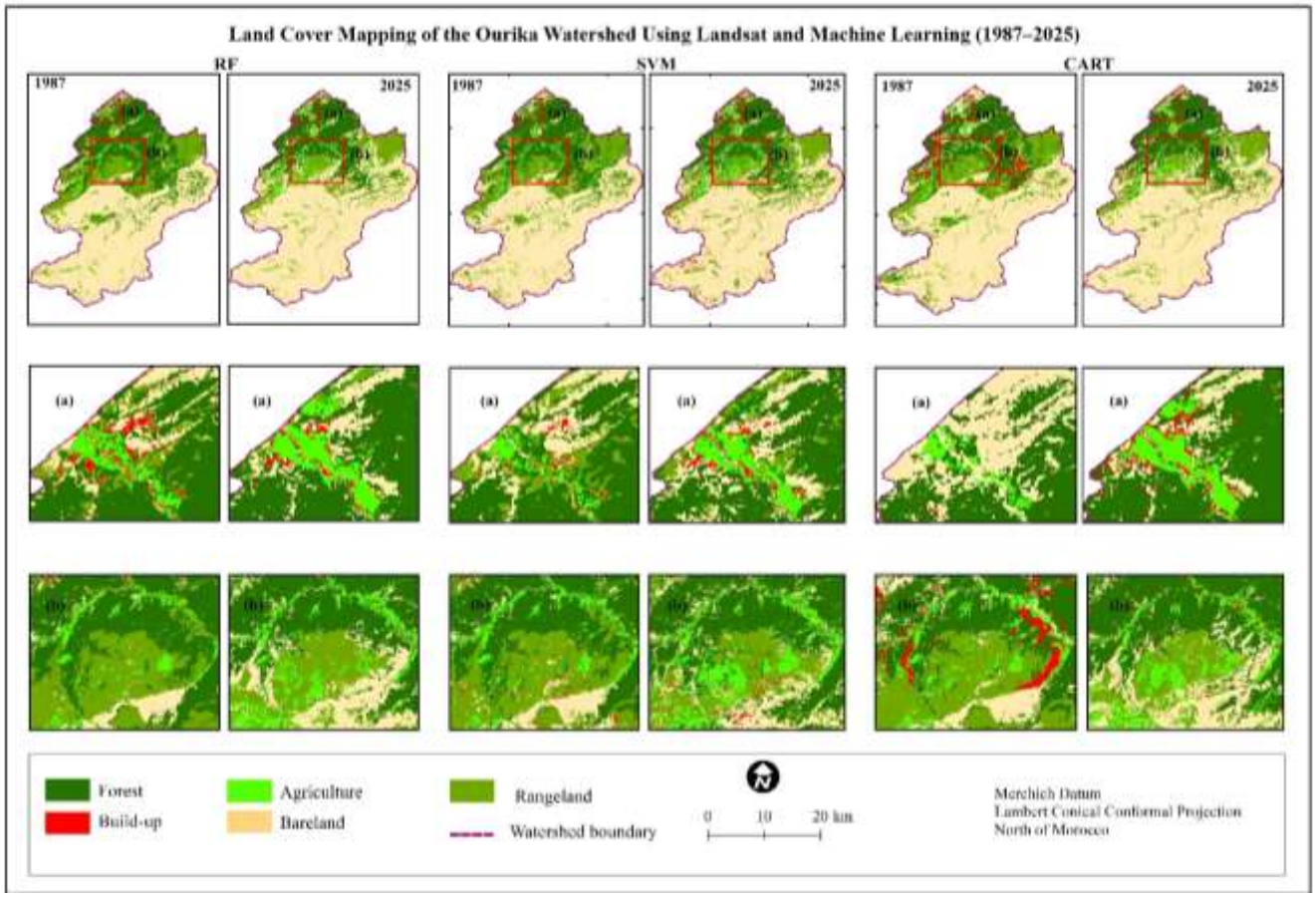

Figure 3. Land cover maps of the Ourika watershed using Landsat images and RF, SVM, and CART classifiers for 1987 and 2025

Overall, the results of the comparison between the classification methods showed that the RF classifier was the most suitable and accurate for classifying land cover in our study area.

3.2. Classification accuracy assessment

An overall accuracy of more than 85% is generally considered satisfactory for LULC classification derived from Landsat imagery [75, 79]. This threshold was surpassed in the present study, indicating that all three machine learning classifiers achieved very good to excellent performance levels.

Classification accuracy refers to the degree of agreement between remote sensing data and reference information [75]. The accuracy assessment in this study relied on four key metrics: Overall Accuracy (OA), Kappa Coefficient (KC), Producer's Accuracy (PA), and User's Accuracy (UA). The corresponding results are summarized in (Table 2) and (Figure 3).

The OA and KC measures (Table 2) showed good performance for the classifiers in general, with a clear superiority of the RF algorithm. In 2025, the RF classifier achieved the highest OA (95%) and KC (0.94), reflecting excellent agreement between the classified and reference datasets. This outcome aligns with previous studies highlighting the robustness of RF in handling nonlinear relationships and spectrally complex datasets [49].

The SVM performed second best for 2025 (OA=90%, KC=0.88), while CART came in third (OA=89%, KC=0.86). A notable improvement in the performance of the SVM classifier can be observed in 2025 compared to 1987, with its overall accuracy jumping from 88% to 90%, which may indicate an improvement in data processing or better parameter fitting. As for performance in 1987, RF maintained its lead (OA=93%, KC=0.91), confirming its robustness even with archival data that may be of lower spectral quality [80].

Table 2. Overall accuracy and Kappa coefficient for the classifiers used

Year	Classfier	Overall Accuracy (%)	Kappa Coefficient
1987	RF	93	0.91
	SVM	88	0.84
	CART	86	0.82
2025	RF	95	0.94
	SVM	90	0.88
	CART	89	0.86

A detailed analysis of accuracy at the category level reveals the precise strengths and weaknesses of each classifier's classification performance (Figure 4). Overall, the RF classifier showed excellent and consistent performance across most categories. In 2025, the PA reached a perfect score (100%) for the bareland class and remained very high (>94%) for all other categories, confirming RF's strong capacity to identify and correctly classify distinct land cover types [46]. Similarly, the extremely high UA (ranging from 93 to 100%) confirms the reliability of the results provided by this classifier, as the points classified within a given category are indeed highly reliable [81].

However, the historical performance (1987) of the build-up class revealed a notable limitation, with a PA of only 40%, meaning that the classifier failed to recognize 60% of the actual build-up areas. This is attributed to the high spectral similarity between built surfaces and rocky surfaces or bareland in mountainous environments in old satellite images with limited spectral and spatial resolution [82].

In contrast, SVM showed a significant improvement in performance within the build-up class between 1987 and 2025. In 2025, product accuracy PA jumped from 40% to 91%, while UA improved from 60% to 87%. This significant shift indicates that SVM's performance is very sensitive to data quality and spectral characteristics, and that with newer and better data, it can compete with RF performance in classifying some difficult categories. This is partly because Landsat 9 OLI data have higher spectral resolution and better-designed bands for distinguishing different surface classes, as well as higher radiometric accuracy (14 bits compared to 8 bits in Landsat 5 TM), which reduces saturation and radiometric clipping and enhances the ability to distinguish between spectrally similar classes, such as built-up areas and bare land. SVM also showed strong and balanced performance across other categories in 2025, with extremely high UA for the bareland category reaching 98%.

In contrast, SVM showed a significant improvement in its performance on the build-up class between 1987 and 2025. In 2025, PA jumped from 40% to 91%, while UA improved from 60% to 87%. This significant shift indicates that SVM's performance is very sensitive to data quality and spectral characteristics, and that with newer and better data, it can compete with RF performance in classifying some difficult categories. It also showed strong and balanced performance across other categories in 2025, with extremely high UA for the bareland category reaching 98%.

The CART classifier performed well but was less reliable than its competitors overall, especially on older datasets. Its main strength was in the UA for the rangeland category, where it scored the highest among the three classifiers for 2025 (97%), meaning that the results it classifies as rangeland are highly reliable. However, challenges persisted with the build-up category, where it scored the lowest PA among the classifiers for 2025 (80%), indicating the difficulty of the tree model in generalizing classification rules for this complex category in the mountainous environment.

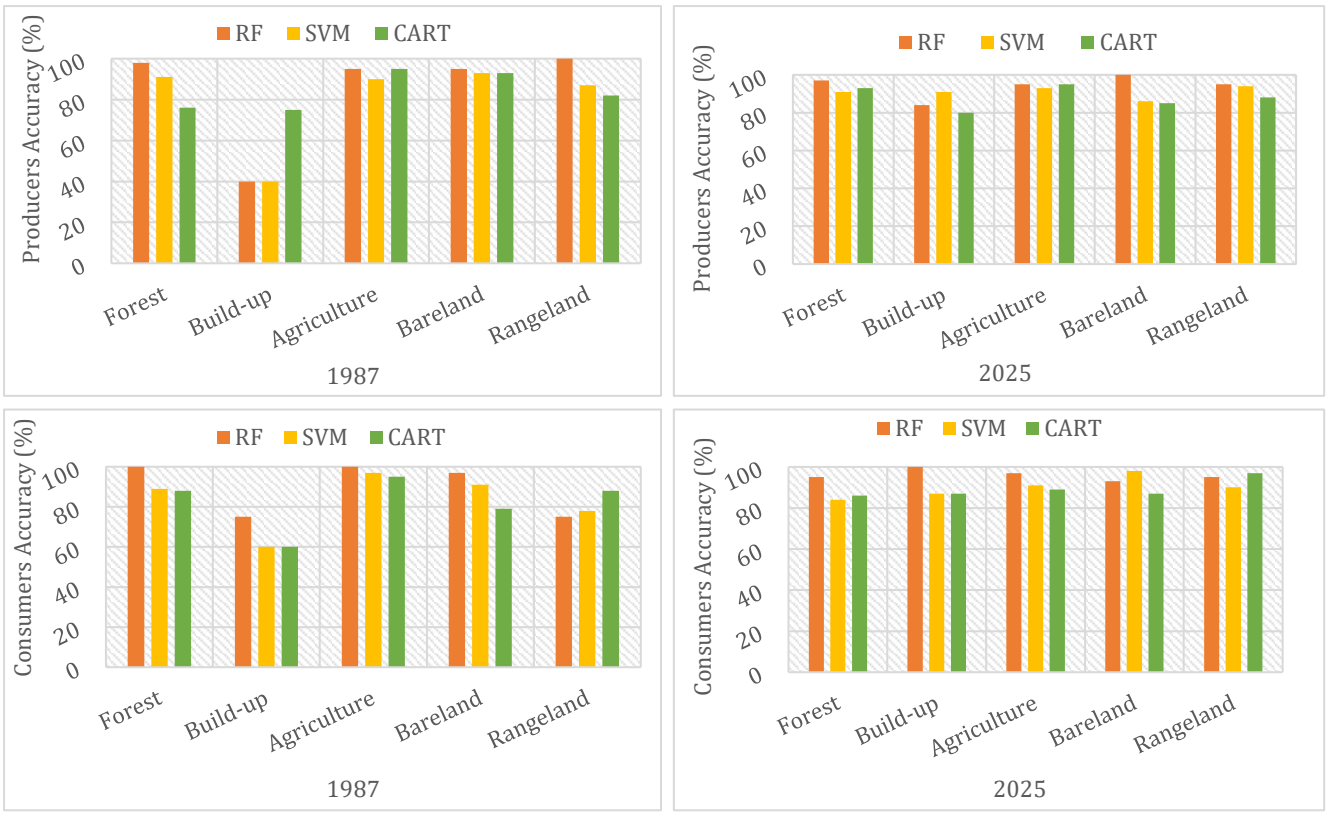

Figure 4. User and producer accuracy for each land cover class of the Ourika watershed using RF, SVM, and CART classifiers

The above analysis confirms the superiority of the RF algorithm as the most reliable and consistent among the classifiers tested in classifying land cover within the Ourika watershed. This result is consistent with what has been shown in the scientific literature in similar contexts [62]. Accordingly, the maps produced using this classification were used as a basis for extracting and calculating the areas specific to each category and determining the patterns of change over time, enabling the study of the impact of these changes on the natural ecosystems of the watershed and the analysis of their dynamics.

3.3. Detecting changes

Mountain ecosystems are widely recognized as global hotspots of environmental change, owing to their high ecological sensitivity to both anthropogenic pressures and climatic variability [83]. (Table 3) and (Table 4) and (Figure 5) present a quantitative assessment of land cover change dynamics within the Ourika watershed, derived from the Landsat-based classifications for 1987 and 2025.

The results highlight profound environmental shifts, with natural ecosystems (forests, rangelands) being lost to agricultural and urban expansion and land degradation, patterns consistent with trends observed in many mountain regions around the world [84, 85]. Although potential changes in land cover have occurred throughout the watershed, most of the direct impact on the study area appears to have been in the vicinity of villages and residential areas.

Table 3. Evolution of the area of land use between 1987 and 2025

	Area				Gain and loss	
Classes	1987 (ha)	1987 (%)	2025 (ha)	2025 (%)	Ha	%
Forest	15032.94	25.94	12232.86	21.11	-2800	-4.83
Agriculture	1623.09	2.8	2490.87	4.3	868	1.5
Rangeland	10021.52	17.29	6990.11	12.06	-3031	-5.23
Buildup	64.52	0.11	170.5	0.29	106	0.18
Bareland	31219.8	53.86	36076.77	62.24	4857	8.38
Total	57961.87	100	57961.11	100	-	-

The data analysis of net land cover change between 1987 and 2025 reveals major transformations across the Ourika watershed. The results indicate three dominant trends: a decline in natural vegetation, a steady human expansion, and a worrisome rise in land degradation.

- **Decline in natural vegetation cover**: Forests experienced the largest net decline recorded to date, falling from 15033 ha (26%) to 12233 ha (21%), corresponding to a net loss of 2800 ha (-4.83% of the total area). Similarly, rangelands experienced a marked decline, falling from 10.022 ha to 6990 ha, reflecting a net loss of 3031 ha (-5.23%). This continued regression reflects the combined influence of deforestation, overgrazing, and agricultural encroachment, which collectively reduce vegetative resilience and accelerate soil exposure and erosion processes [86].
- **Human expansion**: In contrast, the agricultural sector has expanded significantly, increasing from 1623 ha to 2491 ha, representing a net increase of 868 ha (+1.50%). Although the spatial extent of build-up areas is small compared to other major land cover categories, they have experienced relatively significant growth, increasing from 65 ha to 171 ha (0.29%), representing a net increase of 106 ha (+0.18%), which could disproportionately alter the environment when compared to other land use categories.
- **Expansion of land degradation:** Bareland emerged as the most comprehensive and rapidly expanding category, increasing from 31220 ha to 36077 ha (62.24%), indicating an alarming net increase of 4857 ha (+8.38%). This trend is a clear indicator of the degree of land degradation and soil erosion [35].

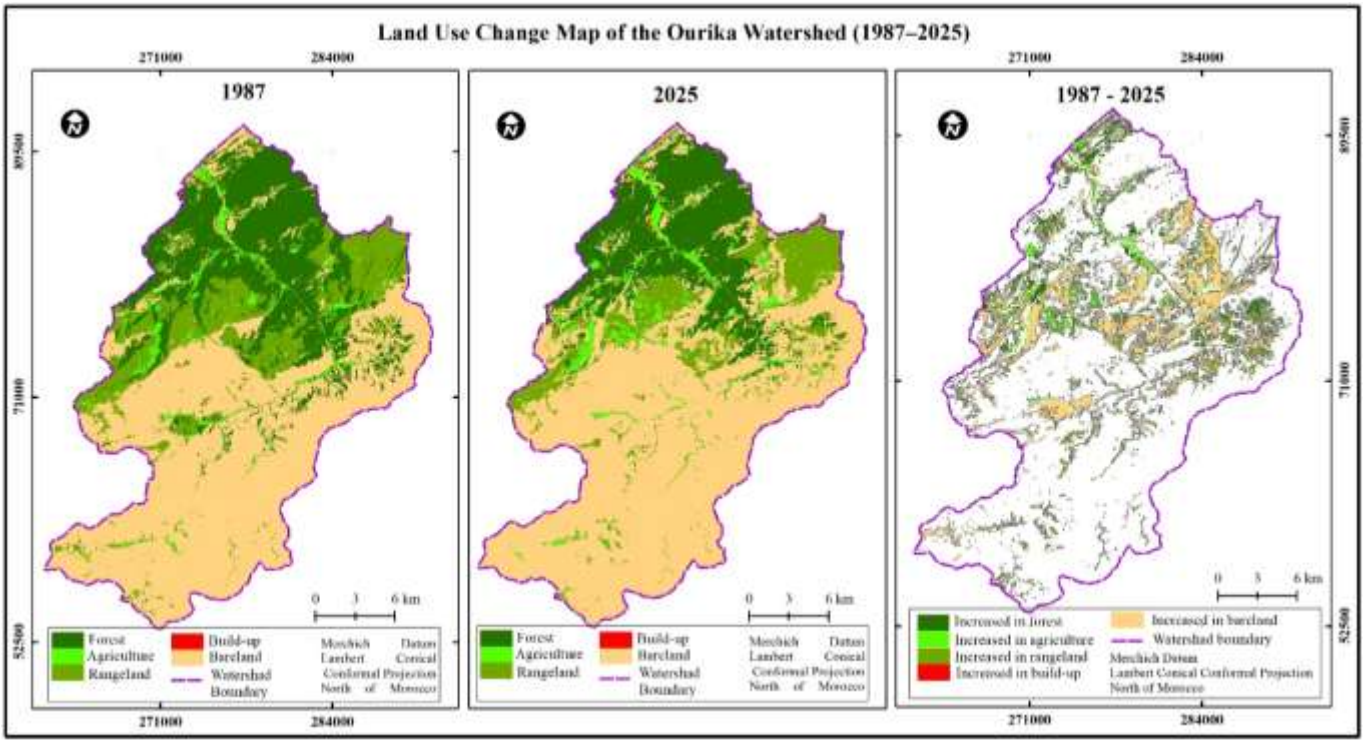

Figure 5. Land use & changes map in the Ourika watershed between 1987 and 2025

Table 4. Matrix of land use change between 1987 and 2025

		2025					
	Classes	Forest	Agriculture	Rangeland	Build-up	Bareland	Total
1987	Forest	10513.24	329.62	683.85	12.76	3464.07	15003.54
	Agriculture	240.62	1181.15	131.61	12.95	56.73	1623.06
	Range land	944.47	830.13	5421.38	68.76	2751.38	10016.12
	Build-up	9.83	14.09	1.16	19.78	19.64	64.5
	Bareland	486.03	135.65	750.21	56.09	29826.67	31254.65
	Total	12194.19	2490.64	6988.21	170.34	36118.49	57961.87

The decrease in forest areas (-2800 ha) alongside the increase in agricultural land (+868 ha) and the increase in bareland (+4857 ha) indicate the conversion and depletion of vegetation cover, either through direct conversion to agricultural use or gradual degradation leading to bare land, as is the case in Amassine, Agadir

Ntamsoult, Sgour, and other areas where the land has deteriorated significantly, creating a badlands. This pattern is consistent with the results of studies showing that agricultural and pastoral pressures and deforestation lead to an increase in degraded and bareland in mountainous areas and their impact on the ecosystem [87].

The vegetation cover of the Ourika watershed is subjected to a combination of natural and anthropogenic factors that accelerate its degradation. On the natural side, climatic variability, recurrent droughts, and intensified soil erosion processes weaken the capacity of ecosystems to recover. In parallel, human-induced pressures—particularly unsustainable land exploitation, overgrazing, and the expansion of agricultural activities beyond the land's biological carrying capacity—have further exacerbated the decline. Together, these drivers have progressively reduced the watershed's regenerative potential, compromising its ecological stability and resilience.

Land change is both a cause and a consequence of global environmental change [38]. The impact of climate change is evident at several levels, most notably the increased variability in precipitation and temperature in the watershed and its impact on the distribution of plant formations and the decline of forested areas. The climate of the watershed is characterized by low summer precipitation and high temperatures. This dry period can be prolonged during the autumn, which is a critical period for plant growth. The low temperatures in winter also pose significant challenges to the survival of both natural and forested vegetation. Furthermore, political and socioeconomic factors affect vegetation cover in conjunction with climate change [87, 88].

The continuous natural increase in population, combined with the fixed size and rugged terrain of the Ourika watershed, the scarcity of arable land, and the prevalence of erosion, are all factors that cause soil loss and push the population to constantly search for new cultivable land, at the expense of forest and pasture areas, to compensate for what they have lost [89]. In this context, the agricultural area expanded by 868 ha during the reference period, and this increase did not come from a single source. It gained 830 ha from pastures, 330 ha from forests, and 136 ha from bareland.

The vegetation formations of the Ourika watershed are thus under severe anthropogenic pressure. The weak economic development, combined with rapid population growth, high unemployment, and widespread poverty, creates a persistent imbalance between human needs and environmental sustainability. Poverty, in particular, drives unsustainable resource exploitation, as local populations depend heavily on forests for fuelwood collection, grazing, construction materials, and charcoal production, often through illegal or informal practices [90]. Such overexploitation undermines the regenerative capacity of forest ecosystems and threatens their long-term ecological functions.

Natural and human factors threatening the vegetation formations in the watershed combine to create a kind of disruption in the natural immune system of trees and fuel attacks by parasites and various diseases that affect plants [38]. During our fieldwork, we observed some manifestations of this phenomenon in groups of pine and cedar forests in the regions of Jamaane and Ait Ammar, green oak forests in Ourir-n-Amouch, and cactus plants in most areas of the watershed.

The Ourika watershed has a number of rangelands that are jointly owned by local tribes, the most important of which are Yagour, Tmenkar, Oukaïmeden, Tifni, and Tenzar. They are exploited and managed by rights holders, and a group of researchers has pointed to the beneficial effects of this community management of rangelands (Agdal) on vegetation cover and the preservation of local biodiversity (flora and fauna), as its protection and controlled use in the spring allow for the reconstitution of plant species [91], which leads to the sustainability of the ecosystem[92]. Despite the area occupied by pastures in the Ourika watershed, their current situation is in constant decline. The (Table 4) shows that more than 2751 hectares of rangelands have been converted to bareland due to harshly changing natural conditions, particularly climatic conditions. During periods of drought, these pastures are often abandoned and opened up several weeks or months early [93], in addition to the pressure resulting from intensive exploitation by rights holders (increased herd numbers).

Qasim et al. (2013) emphasize the strong relationship between road accessibility and land use change, demonstrating a positive correlation between road network density and the rates of deforestation, agricultural expansion, and urban growth. The development of transportation infrastructure facilitates human access to previously remote areas, accelerating land conversion processes and increasing anthropogenic pressure on natural ecosystems [94].

The net increase in build-up areas was relatively small (106 ha), with approximately 69 ha converted from rangeland, 56 ha from bare land, and 13 ha from agricultural land. Although urban areas remain small in absolute terms, the large relative increase (+164%) reflects rural expansion and the creation of new tourist, commercial, and service infrastructure along the river and near road hubs, with accompanying impacts on surface and groundwater balance and quality degradation, especially in areas where there is no wastewater treatment [95]. This could have many negative environmental consequences in the short and long term on the landscape and aesthetics that are the backbone of tourism in the watershed.

The expansion of urban areas on the foothills and along the main course of the river is a key factor in amplifying a range of environmental risks [31], including landslides, erosion, and flooding. It even increases the likelihood of devastating floods, such as the disaster of August 17, 1995, which caused serious human and material losses [33], and the 2014 flood, which also caused significant losses and damage to infrastructure, isolated many residential areas, and flooded much of the agricultural land as a result of a series of water diversion structures at the river level and encroachment on public water property.

The change in land cover from vegetation to urban development affects the local climate of the watershed in what is known as the "urban heat island" effect [31]. The combination of reduced vegetation cover, impervious surfaces, and the shape of buildings in build-up areas reduces evaporative cooling, heat storage, and surface air warming [30, 31, 95, 96]. Zhou et al. (2004) presented evidence of the impact of land cover changes in urban areas on surface temperature in southeastern China [97]. Build-up areas can alter the environment disproportionately when compared to other land use categories.

Continuous changes in land cover, such as the conversion of forest and grassland areas to other types of land cover and vice versa, can greatly increase threats to the watershed's ecosystems.

4. Conclusion and perspectives

The present study aimed to assess the performance of machine learning classifiers in land cover mapping using remote sensing data, with a particular focus on comparing the accuracy of three algorithms RF, CART, and SVM. These classifiers were applied to multispectral datasets from the Landsat 5 and Landsat 9 missions, complemented by various spectral indices and spatial enhancement techniques to optimize classification accuracy.

The results demonstrated that the RF algorithm achieved the highest accuracy and stability in distinguishing land cover categories, confirming its robustness in managing spectral and spatial complexities, particularly within mountainous environments. The temporal analysis covering the period from 1987 to 2025 revealed pronounced environmental transformations, characterized by a decline of approximately 10% in natural areas (forests and rangelands), alongside a continuous expansion of agricultural, urban, and barelands.

The findings highlight that the ecosystems of the Ourika watershed are increasingly subjected to both climatic and anthropogenic pressures. Climatic variability -especially changes in precipitation and temperature -combined with rapid and unregulated human activities, such as agricultural intensification and urban encroachment, have exceeded the ecosystem's natural carrying capacity. This imbalance has accelerated land degradation and reduced the potential for natural regeneration.

From a methodological perspective, this study contributes to the monitoring and quantitative assessment of long-term environmental changes using machine learning and remote sensing. It provides valuable insights for spatial planning, ecosystem restoration, and the sustainable management of fragile mountainous environments.

Future research should aim to identify both the proximate and underlying drivers of land use and land cover change in the Ourika watershed. This can be achieved by integrating field-based household surveys and expert interviews to gather quantitative and qualitative data that elucidate local dynamics and governance-related factors. Additionally, the adoption of advanced machine learning and predictive modelling techniques is recommended to forecast future land use trajectories and support proactive environmental management strategies.

Acknowledgement

This research article was supported by the research group on geography and development at Abdelmalek Essaadi University. We thank all the authors who provided their help and expertise during the field investigation and paper writing. In addition. The authors thank the reviewers for their helpful comments and recommendations.

Author contributions

The authors, **M. Chakouri, H. Chouidda,** validated the document and worked on the design. **A. Jellouli and A. Okacha** contributed to the methodology, and **A. Ouguinaz** reviewed and grouped the ideas and wrote the text of the manuscript.

Conflicts of interest

The authors declare no conflicts of interest.

References

1. Hashem, N., & Balakrishnan, P. (2015). Change analysis of land use/land cover and modelling urban growth in Greater Doha, Qatar. Annals of GIS, 21(3), 233–247. https://doi.org/10.1080/19475683.2014.992369
2. Dapke, P., Quadri, S. A., Nagare, S. M., Bandal, S. B., & Baheti, M. R. (2025). A Comparative Analysis Machine Learning Techniques for LULC Classification Using Landsat-8 Satellite Imagery. International Journal of Engineering and Geosciences, 10(1), 84–92. https://doi.org/10.26833/ijeg.1503104
3. Reis, S. (2008). Analyzing land use/land cover changes using remote sensing and GIS in Rize, North-East Turkey. Sensors, 8(10), 6188–6202. https://doi.org/10.3390/s8106188
4. Wulder, M. A., Loveland, T. R., Roy, D. P., Crawford, C. J., Masek, J. G., Woodcock, C. E., & Cohen, W. B. (2019). Current status of Landsat program, science, and applications. Remote Sensing of Environment, 225, 127–147. https://doi.org/10.1016/j.rse.2019.02.015
5. Sridhar, V., Kang, H., & Ali, S. A. (2019). Human-Induced Alterations to Land Use and Climate and Their Responses for Hydrology and Water Management in the Mekong River Basin. Water, 11(6), 1307. https://doi.org/10.3390/water11061307
6. Sujatha, E. R., & Sridhar, V. (2018). Spatial Prediction of Erosion Risk of a Small Mountainous Watershed Using RUSLE: A Case-Study of the Palar Sub-Watershed in Kodaikanal, South India. Water,

10(11), 1608. https://doi.org/10.3390/w10111608
7. Sridhar, V., & Anderson, K. A. (2017). Human-induced modifications to land surface fluxes and their implications on water management under past and future climate change conditions. Agricultural and Forest Meteorology, 234–235, 66–79. https://doi.org/10.1016/j.agrformet.2016.12.009
8. Paul, S. (2022). Change detection and future change prediction in Habra I and II block using remote sensing and GIS–A case study. International Journal of Engineering and Geosciences, 7(2), 191–207. https://doi.org/10.26833/ijeg.975222
9. Che, T., Xiao, L., & Liou, Y.-A. (2014). Changes in glaciers and glacial lakes and the identification of dangerous glacial lakes in the Pumqu River Basin, Xizang (Tibet). Advances in Meteorology, 2014(1), 903709. https://doi.org/10.1155/2014/903709
10. Sür, İ. B., Algancı, U., & Sertel, E. (2025). Evaluating the performance of deep learning-based segmentation algorithms for land use land cover mapping in a heterogenous vegetative environment. International Journal of Engineering and Geosciences, 10(3), 380–397. https://doi.org/10.26833/ijeg.1528938
11. Badjana, H. M., Helmschrot, J., Selsam, P., Wala, K., Flügel, W., Afouda, A., & Akpagana, K. (2015). Land cover changes assessment using object-based image analysis in the Binah River watershed (Togo and Benin). Earth and Space Science, 2(10), 403–416. https://doi.org/10.1002/2014EA000083
12. Mellor, A., Boukir, S., Haywood, A., & Jones, S. (2015). Exploring issues of training data imbalance and mislabelling on random forest performance for large area land cover classification using the ensemble margin. ISPRS Journal of Photogrammetry and Remote Sensing, 105, 155–168. https://doi.org/10.1016/j.isprsjprs.2015.03.014
13. Zhang, L., Nan, Z., Xu, Y., & Li, S. (2016). Hydrological impacts of land use change and climate variability in the headwater region of the Heihe River Basin, Northwest China. PLoS ONE, 11(6), e0158394. https://doi.org/10.1371/journal.pone.0158394
14. Prenzel, B. (2004). Remote sensing-based quantification of land-cover and land-use change for planning. Progress in Planning, 61(4), 281–299. https://doi.org/10.1016/S0305-9006(03)00065-5
15. Mallinis, G., Koutsias, N., & Arianoutsou, M. (2014). Monitoring land use/land cover transformations from 1945 to 2007 in two peri-urban mountainous areas of Athens metropolitan area, Greece. Science of the Total Environment, 490, 262–278. https://doi.org/10.1016/j.scitotenv.2014.04.129
16. Zhai, R., Zhang, C., Li, W., Zhang, X., & Li, X. (2020). Evaluation of driving forces of land use and land cover change in New England area by a mixed method. ISPRS International Journal of Geo-Information, 9(6), 350. https://doi.org/10.3390/ijgi9060350
17. Avcı, C., Budak, M., Yağmur, N., & Balçık, F. (2023). Comparison between random forest and support vector machine algorithms for LULC classification. International Journal of Engineering and Geosciences, 8(1), 1–10. https://doi.org/10.26833/ijeg.987605
18. Abdulawahid, W., Feizizadeh, B., & Yakar, M. (2025). Integrating Socio-Political Dynamics and Geospatial Machine Learning: An Integrated-Hybrid ANN approach for sustainable Urban Planning in Post-Conflict Baghdad. International Journal of Engineering and Geosciences, 11(2), 408–431. https://doi.org/10.26833/ijeg.1730367
19. Gadal, S., & Mozgeris, G. (2025). Advances of Remote Sensing in Land Cover and Land Use Mapping. Remote Sensing, 17(1980), 2–7. https://doi.org/10.3390/books978-3-7258-5920-7
20. Sandhu, T. H. (2018). Machine Learning and Natural Language Processing - a Review. International Journal of Advanced Research in Computer Science, 9(2), 582. https://doi.org/10.26483/ijarcs.v9i2.5799
21. He, M., Sandhu, P., Namadi, P., Reyes, E., Guivetchi, K., & Chung, F. (2025). Protocols for Water and Environmental Modeling Using Machine Learning in California. Hydrology, 12(3), 59. https://doi.org/10.3390/hydrology12030059
22. Wilkinson, G. G. (2005). Results and implications of a study of fifteen years of satellite image classification experiments. IEEE Transactions on Geoscience and Remote Sensing, 43(3), 433–440. https://doi.org/10.1109/TGRS.2004.837325
23. Alloghani, M., Al-Jumeily, D., Mustafina, J., Hussain, A., & Aljaaf, A. J. (2020). A systematic review on supervised and unsupervised machine learning algorithms for data science. In: Berry, M., Mohamed, A., Yap, B. (eds) Supervised and Unsupervised Learning for Data Science. Supervised and Unsupervised Learning for Data Science, 3–21. https://doi.org/10.1007/978-3-030-22475-2_1
24. Iounousse, J., Er-Raki, S., El Motassadeq, A., & Chehouani, H. (2015). Using an unsupervised approach of Probabilistic Neural Network (PNN) for land use classification from multitemporal satellite images. Applied Soft Computing, 30, 1–13. https://doi.org/10.1016/j.asoc.2015.01.037
25. Hastie, T., Tibshirani, R., & Friedman, J. (2009). Unsupervised Learning. In T. Hastie, R. Tibshirani, & J. Friedman (Eds.), The Elements of Statistical Learning: Data Mining, Inference, and Prediction (pp. 485–585). Springer. https://doi.org/10.1007/978-0-387-84858-7_14
26. Halder, A., Ghosh, A., & Ghosh, S. (2011). Supervised and unsupervised landuse map generation from remotely sensed images using ant

based systems. Applied Soft Computing, 11(8), 5770–5781. https://doi.org/10.1016/j.asoc.2011.02.030

27. Cohen, W. B., Yang, Z., Stehman, S. V., Schroeder, T. A., Bell, D. M., Masek, J. G., & Meigs, G. W. (2016). Forest disturbance across the conterminous United States from 1985–2012: The emerging dominance of forest decline. Forest Ecology and Management, 360, 242–252. https://doi.org/10.1016/j.foreco.2015.10.042
28. Rahman, A., Abdullah, H. M., Tanzir, M. T., Hossain, M. J., Khan, B. M., Miah, M. G., & Islam, I. (2020). Performance of different machine learning algorithms on satellite image classification in rural and urban setup. Remote Sensing Applications: Society and Environment, 20, 100410. https://doi.org/10.1016/j.rsase.2020.100410
29. El Moussaoui, E. H., Moumni, A., Khabba, S., Amazirh, A., Er-Raki, S., Chehbouni, A., & Lahrouni, A. (2025). A comparative methodological approach for argan forest classification using Landsat imagery. Environmental Monitoring and Assessment, 197(2), 210. https://doi.org/10.1007/s10661-025-13649-8
30. Morsy, S., & Hadı, M. (2022). Impact of land use/land cover on land surface temperature and its relationship with spectral indices in Dakahlia Governorate, Egypt. International Journal of Engineering and Geosciences, 7(3), 272–282. https://doi.org/10.26833/ijeg.978961
31. Rahman, H. U., Ding, H., Wang, G., Ullah, S., & Khan, A. (2025). Impacts of Spatio-temporal land use land cover changes on the Development of Urban Heat Islands in a Diverse Topographic Region of District Nowshera, Pakistan. International Journal of Engineering and Geosciences, 11(2), 363–374. https://doi.org/10.26833/ijeg.1763338
32. Elmalki, M., Mounir, F., Ichen, A., Khai, T., & Aarab, M. (2021). A diachronic study of Ourika watershed land in the High Atlas of Morocco. In E3S Web of Conferences, 234, 80. https://doi.org/10.1051/e3sconf/202123400080
33. Saidi, M. E. M., Daoudi, L., El Hassane Aresmouk, M., Fniguire, F., & Boukrim, S. (2010). Les crues de l'oued Ourika (Haut Atlas, Maroc): Événements extrêmes en contexte montagnard semi-aride. Comunicações Geológicas, 97(1), 113–128.
34. Biron, P.-E. (1982). Le Permo-Trias de la région de l'Ourika (Haut Atlas de Marrakech, Maroc): lithostratigraphie, sédimentologie, tectonique et minéralisations. Doctoral dissertation, Université Scientifique et Médicale de Grenoble.
35. Modeste, M., Abdellatif, K., Nadia, M., & Zhang, H. (2016). Impact of land use and vegetation cover on risks of erosion in the Ourika watershed (Morocco). American Journal of Engineering Research (AJER), 5(9), 75–82.
36. Kusi, K. K., Khattabi, A., Mhammdi, N., & Lahssini, S. (2020). Prospective evaluation of the impact of land use change on ecosystem services in the Ourika watershed, Morocco. Land Use Policy, 97, 104796. https://doi.org/10.1016/j.landusepol.2020.104796
37. Ayt Ougougdal, H., Yacoubi Khebiza, M., Messouli, M., & Lachir, A. (2020). Assessment of future water demand and supply under IPCC climate change and socio-economic scenarios, using a combination of models in Ourika Watershed, High Atlas, Morocco. Water, 12(6), 1751. https://doi.org/10.3390/w12061751
38. Song, X.-P., Hansen, M. C., Stehman, S. V., Potapov, P. V., Tyukavina, A., Vermote, E. F., & Townshend, J. R. (2018). Global land change from 1982 to 2016. Nature, 560(7720), 639–643. https://doi.org/10.1038/s41586-018-0411-9
39. Crawford, C. J., Roy, D. P., Arab, S., Barnes, C., Vermote, E., Hulley, G., & Zahn, S. (2023). The 50-year Landsat collection 2 archive. Science of Remote Sensing, 8, 100103. https://doi.org/10.1016/j.srs.2023.100103
40. Masek, J. G., Wulder, M. A., Markham, B., McCorkel, J., Crawford, C. J., Storey, J., & Jenstrom, D. T. (2020). Landsat 9: Empowering open science and applications through continuity. Remote Sensing of Environment, 248, 111968. https://doi.org/10.1016/j.rse.2020.111968
41. Abrams, M., Crippen, R., & Fujisada, H. (2020). ASTER global digital elevation model (GDEM) and ASTER global water body dataset (ASTWBD). Remote Sensing, 12(7), 1156. https://doi.org/10.3390/rs12071156
42. Balcan, M. F., & Sharma, D. (2024). Learning accurate and interpretable decision trees. The 40th Conference on Uncertainty in Artificial Intelligence.
43. Molnar, C., Casalicchio, G., & Bischl, B. (2020). Interpretable Machine Learning – A Brief History, State-of-the-Art and Challenges. In I. Koprinska, M. Kamp, A. Appice, C. Loglisci, L. Antonie, A. Zimmermann, … J. A. Gulla (Eds.), ECML PKDD 2020 Workshops (pp. 417–431). Cham: Springer International Publishing.
44. Nitze, I., Schulthess, U., & Asche, H. (2012). Comparison of machine learning algorithms, random forest, artificial neural network, and support vector machine to maximum likelihood for supervised crop type classification. Proceedings of the 4th GEOBIA, Rio de Janeiro, Brazil, 79, 3540, 35.
45. Mountrakis, G., Im, J., & Ogole, C. (2011). Support vector machines in remote sensing: A review. ISPRS Journal of Photogrammetry and Remote Sensing, 66(3), 247–259. https://doi.org/10.1016/j.isprsjprs.2010.11.001
46. Talukdar, S., Singha, P., Mahato, S., Pal, S., Liou, Y.-A., & Rahman, A. (2020). Land-use land-cover classification by machine learning classifiers for satellite observations—A review. Remote Sensing, 12(7), 1135.
47. Shelestov, A., Lavreniuk, M., Kussul, N., Novikov, A., & Skakun, S. (2017). Exploring Google Earth Engine platform for big data processing:

Classification of multi-temporal satellite imagery for crop mapping. Frontiers in Earth Science, 5, 232994.
48. Zhang, C., Liu, C., Zhang, X., & Almpanidis, G. (2017). An up-to-date comparison of state-of-the-art classification algorithms. Expert Systems with Applications, 82, 128–150.
49. Belgiu, M., & Drăguţ, L. (2016). Random forest in remote sensing: A review of applications and future directions. ISPRS Journal of Photogrammetry and Remote Sensing, 114, 24–31.
50. Rodríguez-Galiano, V. F., & Chica-Rivas, M. (2014). Evaluation of different machine learning methods for land cover mapping of a Mediterranean area using multi-seasonal Landsat images and Digital Terrain Models. International Journal of Digital Earth, 7(6), 492–509.
51. Zhao, H., & Wang, Y. J. (2012). Research on the factors affecting the classification accuracy of ETM remote sensing image land cover/use. Remote Sensing Technology and Applications, 27, 600–608.
52. Nivedita Priyadarshini, K., Kumar, M., Rahaman, S. A., & Nitheshnirmal, S. (2018). A comparative study of advanced land use/land cover classification algorithms using Sentinel-2 data. The International Archives of the Photogrammetry, Remote Sensing and Spatial Information Sciences, 42, 665–670.
53. Loukika, K. N., Keesara, V. R., & Sridhar, V. (2021). Analysis of Land Use and Land Cover Using Machine Learning Algorithms on Google Earth Engine for Munneru River Basin, India. Sustainability, 13(24), 13758. https://doi.org/10.3390/su132413758
54. Thanh Noi, P., & Kappas, M. (2017). Comparison of Random Forest, k-Nearest Neighbor, and Support Vector Machine Classifiers for Land Cover Classification Using Sentinel-2 Imagery. Sensors, 18(1), 18. https://doi.org/10.3390/s18010018
55. Basheer, S., Wang, X., Farooque, A. A., Nawaz, R. A., Liu, K., Adekanmbi, T., & Liu, S. (2022). Comparison of Land Use Land Cover Classifiers Using Different Satellite Imagery and Machine Learning Techniques. Remote Sensing, 14(19), 4978. https://doi.org/10.3390/rs14194978
56. Jia, K., Liang, S., Wei, X., Yao, Y., Su, Y., Jiang, B., & Wang, X. (2014). Land cover classification of Landsat data with phenological features extracted from time series MODIS NDVI data. Remote Sensing, 6(11), 11518–11532.
57. Zhu, Z., Gallant, A. L., Woodcock, C. E., Pengra, B., Olofsson, P., Loveland, T. R., & Auch, R. F. (2016). Optimizing selection of training and auxiliary data for operational land cover classification for the LCMAP initiative. ISPRS Journal of Photogrammetry and Remote Sensing, 122, 206–221.
58. Pflugmacher, D., Rabe, A., Peters, M., & Hostert, P. (2019). Mapping pan-European land cover using Landsat spectral-temporal metrics and the European LUCAS survey. Remote Sensing of Environment, 221, 583–595.
59. Li, C., Wang, J., Wang, L., Hu, L., & Gong, P. (2014). Comparison of classification algorithms and training sample sizes in urban land classification with Landsat thematic mapper imagery. Remote Sensing, 6(2), 964–983.
60. Foody, G. M., & Arora, M. K. (1997). An evaluation of some factors affecting the accuracy of classification by an artificial neural network. International Journal of Remote Sensing, 18(4), 799–810.
61. Persello, C., & Bruzzone, L. (2014). Active and semisupervised learning for the classification of remote sensing images. IEEE Transactions on Geoscience and Remote Sensing, 52(11), 6937–6956.
62. Rodriguez-Galiano, V. F., Ghimire, B., Rogan, J., Chica-Olmo, M., & Rigol-Sanchez, J. P. (2012). An assessment of the effectiveness of a random forest classifier for land-cover classification. ISPRS Journal of Photogrammetry and Remote Sensing, 67, 93–104.
63. Woodcock, C. E., Allen, R., Anderson, M., Belward, A., Bindschadler, R., Cohen, W., & Helmer, E. (2008). Free access to Landsat imagery. Science, 320, 1011.
64. Gorelick, N., Hancher, M., Dixon, M., Ilyushchenko, S., Thau, D., & Moore, R. (2017). Google Earth Engine: Planetary-scale geospatial analysis for everyone. Remote Sensing of Environment, 202, 18–27.
65. Huang, H., Chen, Y., Clinton, N., Wang, J., Wang, X., Liu, C., & Zheng, Y. (2017). Mapping major land cover dynamics in Beijing using all Landsat images in Google Earth Engine. Remote Sensing of Environment, 202, 166–176.
66. Zurqani, H. A., Post, C. J., Mikhailova, E. A., Schlautman, M. A., & Sharp, J. L. (2018). Geospatial analysis of land use change in the Savannah River Basin using Google Earth Engine. International Journal of Applied Earth Observation and Geoinformation, 69, 175–185.
67. Zhu, Z., & Woodcock, C. E. (2012). Object-based cloud and cloud shadow detection in Landsat imagery. Remote Sensing of Environment, 118, 83–94.
68. Tucker, C. J. (1979). Red and photographic infrared linear combinations for monitoring vegetation. Remote Sensing of Environment, 8(2), 127–150.
69. Kennedy, R. E., Yang, Z., & Cohen, W. B. (2010). Detecting trends in forest disturbance and recovery using yearly Landsat time series: 1. LandTrendr—Temporal segmentation algorithms. Remote Sensing of Environment, 114(12), 2897–2910.
70. Xu, H. (2007). Extraction of urban built-up land features from Landsat imagery using a thematic-oriented index combination technique. Photogrammetric Engineering & Remote Sensing, 73(12), 1381–1391.

71. Nguyen, C. T., Chidthaisong, A., Kieu Diem, P., & Huo, L.-Z. (2021). A modified bare soil index to identify bare land features during agricultural fallow-period in southeast Asia using Landsat 8. Land, 10(3), 231.
72. AlAdemomi, A. S., Okolie, C. J., Daramola, O. E., Agboola, R. O., & Salami, T. J. (2020). Assessing the relationship of LST, NDVI and EVI with land cover changes in the Lagos Lagoon environment. Quaestiones Geographicae, 39(3), 111–123.
73. da Silva, V. S., Salami, G., da Silva, M. I. O., Silva, E. A., Monteiro Junior, J. J., & Alba, E. (2020). Methodological evaluation of vegetation indexes in land use and land cover (LULC) classification. Geology, Ecology, and Landscapes, 4(2), 159–169.
74. Jones, J. W. (2015). Efficient wetland surface water detection and monitoring via landsat: Comparison with in situ data from the everglades depth estimation network. Remote Sensing, 7(9), 12503–12538.
75. Manandhar, R., Odeh, I. O. A., & Ancev, T. (2009). Improving the accuracy of land use and land cover classification of Landsat data using post-classification enhancement. Remote Sensing, 1(3), 330–344.
76. Sader, S. A., Ahl, D., & Liou, W.-S. (1995). Accuracy of Landsat-TM and GIS rule-based methods for forest wetland classification in Maine. Remote Sensing of Environment, 53(3), 133–144.
77. Yu, X., Lu, D., Jiang, X., Li, G., Chen, Y., Li, D., & Chen, E. (2020). Examining the roles of spectral, spatial, and topographic features in improving land-cover and forest classifications in a subtropical region. Remote Sensing, 12(18), 2907.
78. Margono, B. A., Bwangoy, J.-R. B., Potapov, P. V., & Hansen, M. C. (2014). Mapping wetlands in Indonesia using Landsat and PALSAR data-sets and derived topographical indices. Geo-Spatial Information Science, 17(1), 60–71.
79. Anderson, J. R. (1976). A land use and land cover classification system for use with remote sensor data (Vol. 964). US Government Printing Office.
80. Maxwell, A. E., Warner, T. A., & Fang, F. (2018). Implementation of machine-learning classification in remote sensing: An applied review. International Journal of Remote Sensing, 39(9), 2784–2817.
81. Foody, G. M. (2020). Explaining the unsuitability of the kappa coefficient in the assessment and comparison of the accuracy of thematic maps obtained by image classification. Remote Sensing of Environment, 239, 111630.
82. Myint, S. W., Gober, P., Brazel, A., Grossman-Clarke, S., & Weng, Q. (2011). Per-pixel vs. object-based classification of urban land cover extraction using high spatial resolution imagery. Remote Sensing of Environment, 115(5), 1145–1161.
83. Chakraborty, A. (2021). Mountains as vulnerable places: a global synthesis of changing mountain systems in the Anthropocene. GeoJournal, 86(2), 585–604.
84. Grêt-Regamey, A., Brunner, S. H., & Kienast, F. (2012). Mountain ecosystem services: who cares? Mountain Research and Development, 32(S1).
85. Payne, D., Spehn, E. M., Snethlage, M., & Fischer, M. (2017). Opportunities for research on mountain biodiversity under global change. Current Opinion in Environmental Sustainability, 29, 40–47.
86. Modeste, M., Abdellatif, K., Nadia, M., & Mohamed, S. (2018). Effects of land use and cover type on the risks of runoff and water erosion: infiltration tests in the Ourika watershed (High Atlas, Morocco). Euro-Mediterranean Journal for Environmental Integration, 3(1), 8.
87. Winkler, K., Fuchs, R., Rounsevell, M., & Herold, M. (2021). Global land use changes are four times greater than previously estimated. Nature Communications, 12(1), 2501. https://doi.org/10.1038/s41467-021-22702-2
88. Hansen, M. C., Potapov, P. V., Moore, R., Hancher, M., Turubanova, S. A., Tyukavina, A., & Loveland, T. R. (2013). High-resolution global maps of 21st-century forest cover change. Science, 342(6160), 850–853.
89. Tarolli, P., & Straffelini, E. (2020). Agriculture in Hilly and Mountainous Landscapes: Threats, Monitoring and Sustainable Management. Geography and Sustainability, 1(1), 70–76. https://doi.org/10.1016/j.geosus.2020.03.003
90. DREFLCD. (2002). Étude d'aménagement de la forêt de l'Ourika : Étude préliminaire. D. régionale des E. et F. et de lutte contre la désertification, Ed., 54.
91. Alaoui Haroni, S., Alifriqui, M., & Simonneaux, V. (2009). Recent dynamics of the wet pastures at Oukaimeden plateau (High Atlas mountains, Morocco). Biodiversity and Conservation, 18(1), 167–189.
92. Mahdi, M. (2010). Patrimonialisation de la transhumance à l'Oukaïmeden. Pastoralisme méditerranéen: patrimoine culturel et paysager et développement durable, 73.
93. Ramou, H. (2012). Les igudlan n-Izlan (Imilchil). Modalités de gestion et mutations. Agdal. Patrimoine socio-écologique de l'Atlas marocain, Rabat, IRD-Ircam (éd.), 469–488.
94. Qasim, M., Hubacek, K., & Termansen, M. (2013). Underlying and proximate driving causes of land use change in District Swat, Pakistan. Land Use Policy, 34, 146–157. https://doi.org/10.1016/j.landusepol.2013.02.008
95. Foley, J. A., DeFries, R., Asner, G. P., Barford, C., Bonan, G., Carpenter, S. R., & Gibbs, H. K. (2005). Global consequences of land use. Science, 309(5734), 570–574.
96. Ambreen, H., & Rahman, A. (2025). Evaluating Spatio-temporal Dynamics in LULC and its Implications on Land Surface Temperature of Swat valley, Eastern Hindukush. International Journal of Engineering and Geosciences, 10(3), 495–503.

97. Zhou, L., Dickinson, R. E., Tian, Y., Fang, J., Li, Q., Kaufmann, R. K., & Myneni, R. B. (2004). Evidence for a significant urbanization effect on climate in China. Proceedings of the National Academy of Sciences, 101(26), 9540–9544. https://doi.org/10.1073/pnas.0400357101